analytical chemistry

pubs.acs.org/ac Article

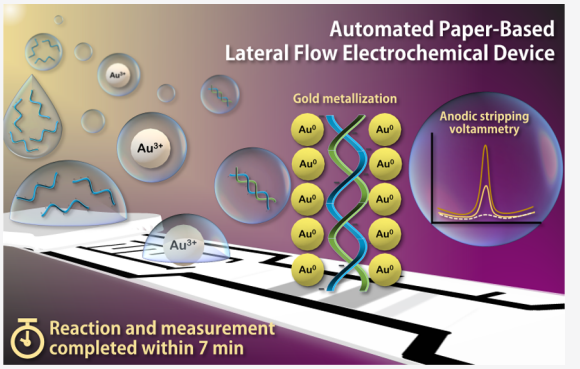
Amplification-free DNA Sensor for the One-Step Detection of the Hepatitis B Virus Using an Automated Paper-Based Lateral Flow Electrochemical Device

Chawin Srisomwat, Abdulhadee Yakoh, Natthaya Chuaypen, Pisit Tangkijvanich, Tirayut Vilaivan, and Orawon Chailapakul*

Cite This: https://dx.doi.org/10.1021/acs.analchem.0c04283 Read Online

ACCESS | Metrics & More | Article Recommendations | Supporting Information

ABSTRACT: Until now, an electrochemical lateral flow assay (eLFA) capable of detecting nucleic acids has remained a challenge and has been scarcely explored because of its complicated multistep nature. Here, we report an automated paper-based eLFA device for the quantitative detection of the hepatitis B virus (HBV)—the major cause of liver cirrhosis and hepatocellular carcinoma (HCC). Using a time-delayed microfluidic strategy fabricated on paper, an automated and precisely sequenced solution transfer was enabled by single sample loading. A gold metallization strategy was employed for the signal-on electrochemical detection of the target DNA. Furthermore, a pyrrolidinyl peptide nucleic acid (so-called "acpcPNA") was used as a probe in this study because it offers higher specificity and yields lower background currents than those of traditional probes. Under optimal conditions, a broad dynamic range (10 pM to 2 μM) with an excellent detection limit (down to 7.23 pM) was achieved. The overall operation can be completed within 7 min of sample loading. The proposed sensor was successfully applied in HBV DNA detection in sera from patients without any amplification step (e.g., PCR) required, thus simplifying the operation further. Additionally, the results obtained from this present device are in accordance with the standard real-time PCR, thus supporting the accuracy of the method.



Downloaded via UNIV OF GOTHENBURG on December 17, 2020 at 12:14:59 (UTC).
See https://pubs.acs.org/sharingguidelines for options on how to legitimately share published articles.

For decades, the lateral flow assay (LFA) has been widely used in many point-of-care (POC) testing devices for qualitative screening of myriads of compounds.[1−3] Its popularity can be attributed to its rapidness, one-step analysis, low cost, user friendliness, and portability.[4] Although many LFA devices have been developed, some limitations of traditional LFA devices remain an issue. One obvious limitation is the inability of the device to perform commonly used sequential multistep biological assays, such as the enzyme-linked immunosorbent assay (ELISA), immunoassay, or even DNA assay.[5] To enable this functionality, manual fluidic manipulation by the user is generally required, which complicates operation.[5] To achieve full automation, three-dimensional LFA devices integrating different functionalities within a single platform have been proposed and applied for immunosensing applications. One of the demonstrations for an automated sandwich LFA-ELISA was developed by Preechakasedkit et al.,[6] In this work, a novel wax-printed channel on a paper-based LFA device was developed to enable timed-sequence reagent delivery and delay the release of the final reagent. Although several automatic LFA platforms for multiple procedures have already been successfully engineered, these systems have been entirely utilized for a qualitative screening application with a yes/no-type colorimetric response. Electrochemical detection, on the other hand, offers both qualitative and quantitative information with excellent sensitivity. Therefore, the implementation of miniaturized electrochemical detectors for LFA is of interest. However, so far, only a few reports for such integrated lateral flow device electrochemical sensors have been published.[7−9] None of these reports have demonstrated the ability for automated multistep assays. Hence, we sought to design and fabricate a sensitive, selective, quantitative, and autonomous approach for DNA assay based on a hybrid LFA electrochemical device.

Herein, an integrated electrochemical LFA (eLFA) device was demonstrated as a point-of-care (POC) diagnostic device for hepatitis B virus (HBV). Chronic hepatitis B infection is a life-threatening and leading cause of fibrosis, cirrhosis, and

Received: October 12, 2020
Accepted: December 7, 2020

© XXXX American Chemical Society

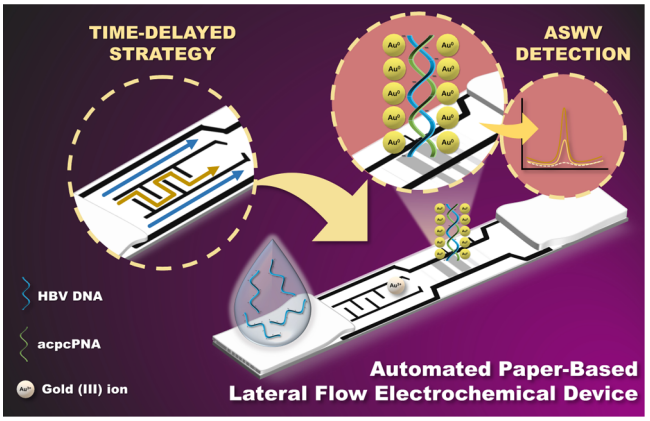
https://dx.doi.org/10.1021/acs.analchem.0c04283
Anal. Chem. XXXX, XXX, XXX−XXX

hepatocellular carcinoma (HCC).[10] Typically, the assessment of serological markers [(hepatitis B surface (HBsAg), antibody to HBs (anti-HBs), hepatitis B e-antigen (HBeAg), anti-HBe, and hepatitis B core antibodies (anti-HBc) IgM and IgG] and nucleic acid (HBV DNA) are routinely used to identify HBV infection, which allows for further monitoring of disease progression.[11] The DNA-based assay for HBV has gained more popularity in clinical medicine recently because of the increasing prevalence of negative serology for HBV infection.[12] Moreover, HBV DNA can be detected at the early stage of infection and is a reliable marker of viral replication activities.[13] Although various nucleic acid detection techniques, for example, Northern and Southern blotting,[14] polymerase chain reaction (PCR) followed by gel electrophoresis, and real-time PCR[15,16] have been demonstrated, their main drawbacks, including the need for specialized equipment, highly trained personnel, and a time-consuming procedure, limit their usefulness outside laboratories. Without the aforementioned limitations, the eLFA platform can, therefore, hold considerable potential as a practical and cost-effective POC diagnostic device for HBV DNA.

Concerning the electrochemical detection of nucleic acids, two different approaches of signal visualization exist: (i) signal off and (ii) signal on. In the signal-off approach, the current response of the mediator/reporter (usually $[Fe(CN)_6]^{3-/4-}$ in the label-free system or methylene blue in the labeled system) decreases upon DNA hybridization as the rigidified structure of the DNA duplex hinders electron transfer between the electroactive reporter and the electrode.[17] In contrast, the current response in the signal-on approach is increased upon DNA duplex formation. This can be achieved by, for example, metallization of DNA. For instance, as reported by Wang et al.,[18] a positively charged silver mediator (Ag^+) added after complete DNA hybridization is accumulated by the high density of negative charges in the phosphate backbone of the DNA structure, which leads to an increase in electron transfer between the electrode and the mediator. From an analytical perspective, the signal-off approach has two major limitations, including a limited signaling capacity to a maximum of 100% signal suppression[19] and a high background signal, which impedes its application in trace-level detection.[20] Therefore, the signal-on approach via metallization, which is not subjected to the same limitations, was chosen in this current work as the sensing scheme. Although additional washing steps (to remove the unbound mediator) are inherently inevitable, an automated and one-step eLFA platform can provide a potential solution for this problem.

In this present work, we have developed a paper-based lateral flow electrochemical DNA sensor that allows time-sequenced reactions to be operated in an automated fashion. The high-performance pyrrolidinyl peptide nucleic acid (also known as acpcPNA) was selected as the recognition probe in this work to capture HBV DNA because it demonstrates a stronger binding affinity toward complementary DNA compared to conventional DNA and PNA probes.[21] Gold ions (Au^{3+}) were specifically selected for the metallization process to avoid silver precipitation (AgCl) in the PBS media generally used for DNA work. To be highlighted, the use of an electrostatically neutral PNA probe should minimize the background current because of the absence of interaction between the PNA probe and Au^{3+} unless the DNA target is present.[20,22,23] The eLFA device was designed to allow full automation as follows: using a printed-delayed configuration, as conceptually shown in Scheme 1, sequential reagent delivery is automatically enabled once the sample is introduced. The sensing platform contains a straight nondelayed channel, a zigzag delayed channel, and a detection zone. In this configuration, the acpcPNA probe is immobilized on the detection zone of the test strip where an electrode is placed underneath, while the Au^{3+} for gold metallization is predeposited at the delayed channel zone. When the sample containing the HBV DNA is loaded, the solution will rapidly move across the nondelayed channel and hybridize with the acpcPNA probe at the detection zone. Meanwhile, the solution flowing through the delayed channel will be retarded by the wax-printed barriers and gradually merge with the preceding flow from the nondelayed channel. Taking advantage of this differential flow behavior, DNA hybridization will occur first, followed by Au^{3+} binding to the captured DNA through electrostatic interactions. The two steps of the assay proceed automatically and sequentially following the sample application and the buffer flow without the requirement of additional solution manipulation or washing steps. For further analysis, an electrochemical reduction deposition was carried out to form the Au^0-metallized DNA, followed by an anodic stripping voltammetry (ASWV) assay to determine the HBV DNA concentration via the gold signal. The overall assay can be completed within 7 min, illustrating a rapid analysis without compromising sensitivity and selectivity. Moreover, this developed sensor shows an excellent capability for real sample analysis using unamplified DNA from patients and demonstrates comparable results with the standardized quantitative PCR (real-time PCR) method. Therefore, the automated eLFA device outlined here offers strong potential for highly sensitive, selective, and rapid DNA analysis with reliable accuracy.

Scheme 1. Schematic Illustration of the eLFA Device for One-Step HBV DNA Detection



EXPERIMENTAL SECTION

Materials, Equipment, and Chemicals. The detail of reagents, electrode inks, synthetic nucleotides, and all electrochemical measurement are illustrated in the Supporting Information.

Synthesis of the acpcPNA Probe. A sequence of the acpcPNA probe (TCC TGG AAT TAG AGG; written in the N → C direction) was designed to be complementary with the HBV DNA target.[24] The acpcPNA probe was synthesized manually on Tentagel S-RAM resin from the respective Fmoc-

https://dx.doi.org/10.1021/acs.analchem.0c04283
Anal. Chem. XXXX, XXX, XXX−XXX

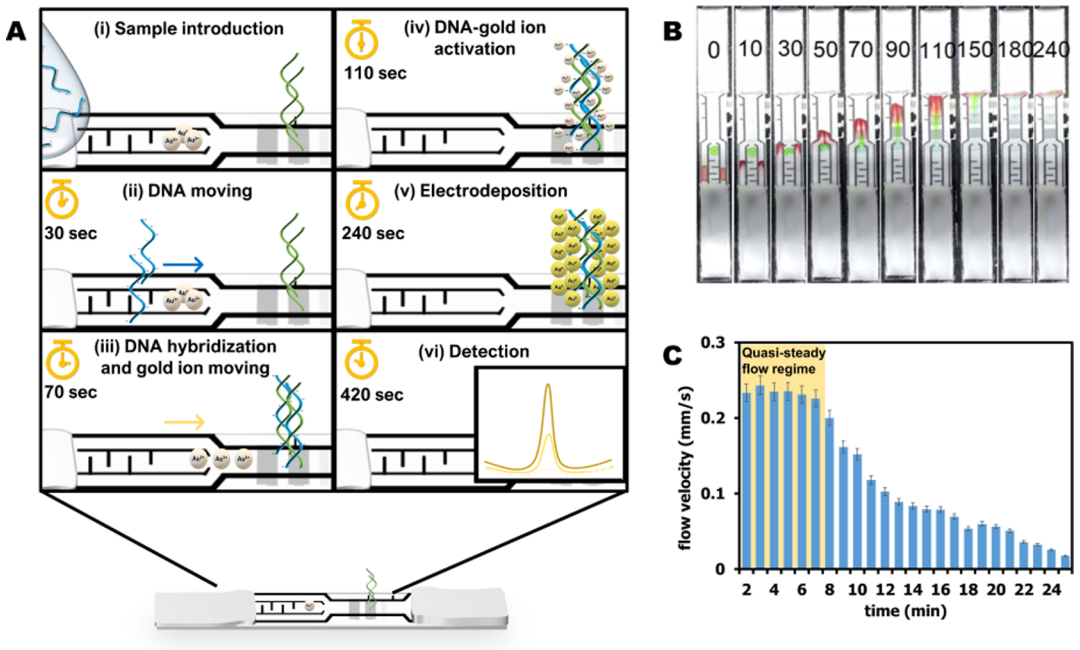


Figure 1. (A) Operation of HBV DNA detection via metallization assay on the automated eLFA device. (B) Solution flow on the device from 0 to 240 s. (C) Plot of flow velocity at different times (from 2 to 25 min). Error bars indicate the standard deviation of flow velocity from three independent devices (n = 3).

protected monomers (A^{Bz}, C^{Bz}, T, and G) and spacer (ACPC) at a 1.5 μmol scale following the literature procedure.[25] The details of the synthesis of the acpcPNA probe are illustrated in the Supporting Information.

Fabrication of the Automated Paper-Based Lateral Flow Device. The design of the automated paper-based lateral flow device for the detection of HBV DNA is shown in Figure S3. The device components consist of a sample pad, wax-printed pad, screen-printed electrode, and an absorbent pad. The pattern of the wax-printed pad was created using Adobe Illustrator CC (Adobe Systems, USA). The designed pattern was printed onto the nitrocellulose membrane using a wax printer (Xerox ColorQube 8570, Japan). Then, the nitrocellulose membrane was placed in an oven at 100 °C for 1 min to create the wax barriers. Three electrodes were screen-printed onto a PVC substrate with the screen-printing technique and dried at 55 °C for 30 min. The screen-printed electrode was assembled on a plastic backing sheet followed by the wax-printed pad, sample pad, and adsorbent pad.

DNA Metallization and Detection. A 0.25 μL aliquot of the acpcPNA probe at a specified concentration was drop-casted onto the detection zone of the wax-printed nitrocellulose pad and baked at 37 °C for 30 min. Next, 0.5 μL of the gold(III) ion at a specified concentration was spotted in the wax-delayed zone (see Scheme 1) and allowed to dry at RT for 5 min. To begin the assay, a solution of the HBV DNA oligonucleotide (or DNA samples from patients) (50 μL) was introduced to the sample pad. After the solution was allowed to flow for 5 min, electrochemical detection was initiated by applying a potential of −0.2 V (vs Ag/AgCl) for 120 s to affect metallization. This was followed by anodic stripping square wave voltammetry (ASWV) in the potential range between 0.2 and 1.2 V (vs Ag/AgCl) to measure the gold signal.

Serum Extraction for HBV DNA. Clinical serum samples were collected at Center of Excellence in Hepatitis and Liver Cancer, Department of Biochemistry, Faculty of Medicine, Chulalongkorn University (Thailand), and extracted for HBV DNA. This study was conducted in compliance with the Helsinki Declaration and Good Clinical Practice guidelines and approved by the Institutional Review Board of the Faculty of Medicine, Chulalongkorn University, Bangkok, Thailand (IRB. no. 050/63). Written informed consent was obtained from all patients for the use of their clinical data and sample specimens. The DNA samples were extracted using the phenol−chloroform−isoamyl alcohol method. The details for this method are demonstrated in the Supporting Information.

The standard curve for HBV DNA was produced by serial dilution of a plasmid HBV genome (pUC19-pHBV, provided by the Department of Virology and Liver Unit, Graduate School of Medical Sciences, Nagoya City University, Japan) to a concentration of 10^2 to 10^9 copies/μL. Details of the plasmid preparation are illustrated in the Supporting Information.

Virological Assays. Quantitation of the HBV DNA level in the serum was by an in vitro polymerase chain reaction (PCR) assay employing a commercially available Abbott RealTime HBV assay kit (Abbott Laboratories) as a standard assay for HBV DNA detection.

RESULTS AND DISCUSSION

Device Design and Operation. In this part, the sensing scheme and functions of the device are discussed. To develop the eLFA device for a time-sequenced reaction triggered by a single sample loading, a paper test strip containing three distinct fluidic channels was fabricated using the wax-printing method. Here, the nitrocellulose (NC) test strip with dimensions of 6 × 55 mm comprises a straight nondelayed channel for sample delivery, a zigzag delayed (baffle) channel for Au^{3+} delivery, and a trapezoid-shaped detection zone for the detection step. The acpcPNA probe was immobilized on the NC at the detection zone via hydrophobic interactions. This PNA-loaded printed NC paper was then assembled with other LFA components (screen-printed electrode, sample pad,

https://dx.doi.org/10.1021/acs.analchem.0c04283
Anal. Chem. XXXX, XXX, XXX−XXX

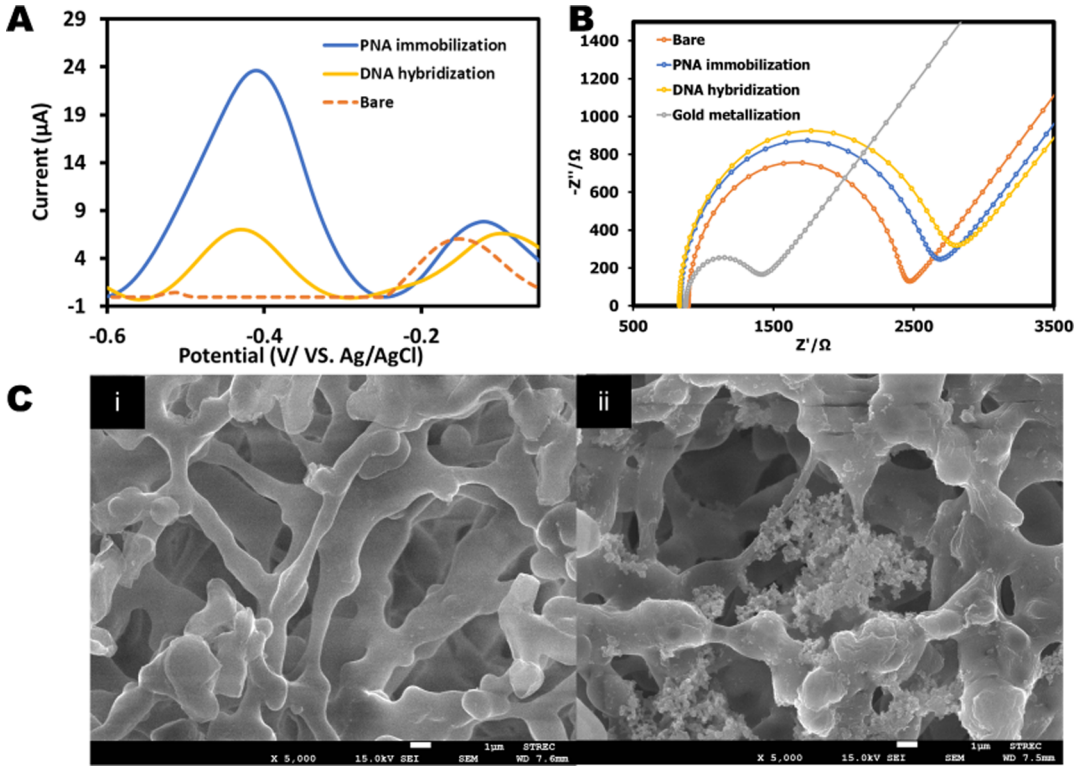


Figure 2. Characterization of the HBV DNA detection for the proposed device. (A) DPVs using methylene blue as an electrochemical reporter tested with a bare electrode (dotted orange line) and an acpcPNA immobilized electrode before (blue line) and after (yellow line) DNA hybridization. The peak at −0.1 V vs Ag/AgCl is due to SDS. (B) Nyquist plots from each step of DNA detection, including acpcPNA immobilization, DNA hybridization, and gold metallization. (C) SEM images of a bare lateral flow test strip (i) and after gold metallization by electrodeposition (ii).

and adsorbent pad) onto a plastic backing card, as illustrated in Figure S3. Taking advantage of this device design, the different reagent flow times between the delayed and nondelayed channels enable sequential reagent delivery. As conceptually represented in Figure 1A, once the sample is introduced (i), the complementary target DNA will rapidly traverse across the nondelayed fluidic channel (ii) and reach the detection zone. Here, the arriving target DNA will hybridize with the complementary PNA probe, and, thus, immobilize (iii), while that moving through the baffle barrier in the delayed channel will be slowed down and subsequently merged with the main fluidic stream from the nondelayed channel. This slower flow will carry the prespotted metallizing reagent (Au^{3+}) from the delayed channel to the detection zone. Here, the interaction (mainly electrostatic and coordination)[26] between the Au^{3+} and the phosphate backbone of the immobilized DNA (iv) occurs. At this stage, the overflowing sample and Au^{3+} will be washed out by the continuous fluid stream. Next, a negative reduction potential is applied to deposit Au^0 in the form of gold nanoparticles (AuNPs) (v). Finally, square-wave voltammetry is conducted to analyze the gold-metallized DNA (vi). This multistep procedure can be accomplished within 7 min following the addition of a single drop (50 μL) of the sample.

To demonstrate the sequential fluid delivery of the proposed eLFA device, red and green dyes representing the target DNA and Au^{3+} were separately spotted onto the nondelayed and delayed zones, respectively (Figure 1B). After loading the buffer solution, the solution passing through the nondelayed paths immediately eluted the red-colored spot, while the solution flowing through the delayed path required a longer time (~30 s) to reach the green spot. Additionally, it was clearly observed that the red fluidic front entered the detection zone (where the electrode was placed underneath) within 70 s, while the green fluidic front required 110 s to reach the same spot. In addition, both dyes were visibly rinsed off to the absorbent pad within 240 s, indicating the capability of the device to transfer the sample and the reagent automatically in a time-sequenced fashion. A video of the solution flow on the proposed device is shown in Movie S1.

Characterization of the Flow Behavior on the Automated Paper-Based Lateral Flow Device. Generally, electrochemical detection on paper-based analytical devices (PADs) is performed in a quiescent solution.[27] Only a few studies have been reported under hydrodynamic conditions.[28] The convective solution flow significantly impacts the electrochemical response. The increase in mass transport due to convection in a continuous flow system (aside from diffusion contribution in the static system) generally leads to a higher current response.[29] Therefore, it is important to investigate the flow behavior (flow velocity and amperometric response) within the eLFA device.

First, the flow velocity was visually characterized by measuring the time for the Milli-Q water to traverse through the nondelayed and delayed zone and dissolve the color dye spotted at the bottleneck of the detection channel until it reached the test zone (Movie S2). The application of the color droplets was repeated in 1 min intervals until the flow from the carrier solution terminated or the fluid front of the color dye was no longer separated from the previous color band (~25

https://dx.doi.org/10.1021/acs.analchem.0c04283
Anal. Chem. XXXX, XXX, XXX−XXX

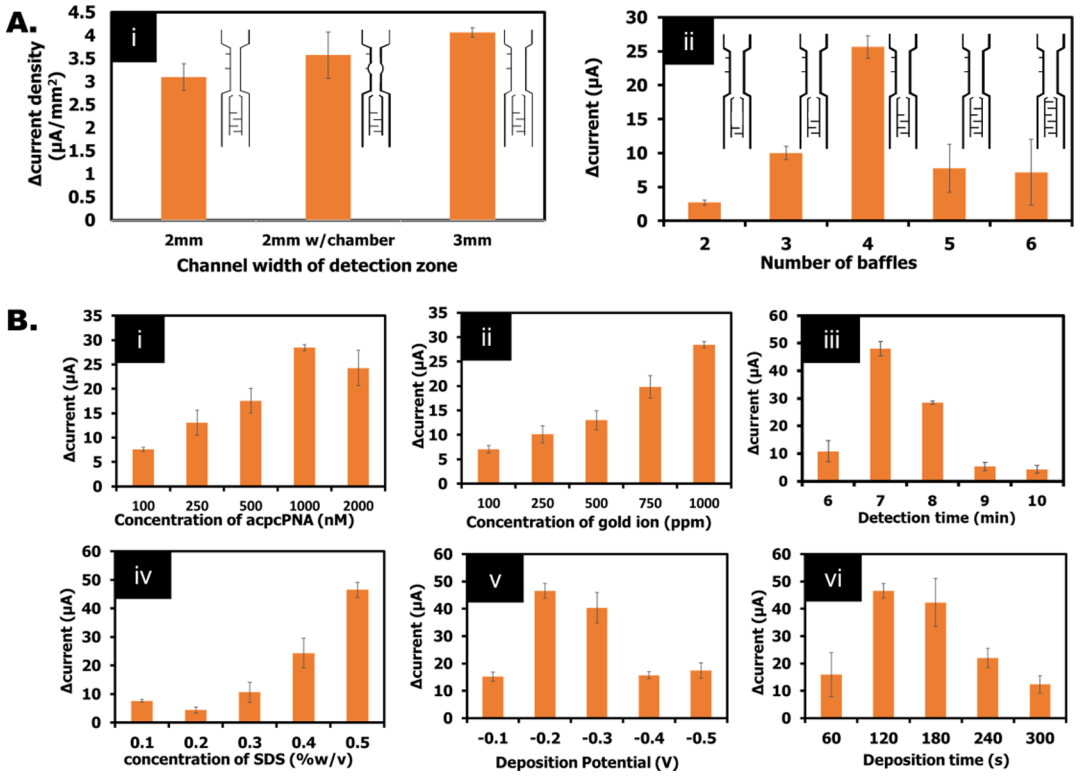


Figure 3. Optimization of the important parameters for HBV DNA detection including (A) influence of device geometry, (i) channel width of the detection zone and (ii) the number of baffles, and (B) assay conditions; (i) concentration of acpcPNA, (ii) concentration of the gold ion, (iii) detection time, (iv) concentration of SDS, (v) deposition potential, and (vi) deposition time. Error bars indicate the standard deviation of the differential current for three independent devices (n = 3). Note that an HBV target DNA concentration of 2 μM was used for the whole optimization.

min). As summarized in Figure 1C, a steady flow velocity of 0.23 ± 0.02 mm s^{-1} was maintained up to 7 min, corresponding to a quasi-steady flow within the analysis channel.[28] After that, a gradual decrease in flow velocity was observed, which can be described by the Lucus−Washburn equation.[30]

$$l(t) = \sqrt{\left(\frac{\gamma r \cos\theta}{2\mu}\right)t} \quad (1)$$

According to eq 1, the distance the fluidic front flows through with time ($l(t)$) is directly proportional to the square root of time (t) as the solution surface tension (γ), effective pore radius of the paper (r), cosine of the solution contact angle (θ), and viscosity (μ) are constant.[30]

At the initial time, the linear relationship between the distance and time showed a constant slope (or constant flow velocity), providing a quasi-steady flow behavior. After the steady-flow regime, the slope decreased and approached zero, demonstrating the decline in the rate of flow, and eventually stopped at a certain time. The theoretical explanation can, thus, satisfactorily describe the experimental results.

Furthermore, an additional chronoamperometric detection experiment was also conducted. Instead of the dyes, an electroactive species (L-ascorbic acid; AA) was continuously introduced every 2 min at the beginning of the detection channel to study the current response (Figure S4). From the amperometric i−t curve, it was observed that the current responses showed identical feedback (peak width of 60 s; peak height (peak current) of 32.8 nA with % RSD of 13.9; and peak area (charge) of 1.06 μC with % RSD of 5.74) within the quasi-steady regime (2−7 min). This complementary result clearly supports the previous flow velocity investigation, whereby a constant velocity was obtained within the quasi-steady regime. The current responses of the AA at the transient state (>7 min) yielded overlapping peaks with a broadening of the peak width. This result can be explained by the decrease in flow rate over time within the porous paper device. All things being considered, the analytical experiment was, therefore, performed under the quasi-steady flow regime to maintain a uniform flow velocity.

Characterization of the Gold-Metallized DNA Complex. To investigate the applicability of DNA detection on the eLFA device, acpcPNA probe immobilization and subsequent hybridization with complementary target DNA were electrochemically characterized with differential pulse voltammetry (DPV) and electrochemical impedance spectroscopy (EIS) techniques. Herein, methylene blue (MB) with a concentration of 20 μM in Milli-Q water, which can bind with DNA via guanine bases and intercalation, was used as a redox indicator to monitor the hybridization between the acpcPNA probe and the complementary DNA target.[31,32] Figure 2A illustrates the differential pulse voltammograms for the reduction signal of the MB indicator. In the continuous flow system, no peak due to MB was observed (orange line) on the bare electrode (non-immobilized). After the acpcPNA was immobilized on the detection zone, the appearance of the MB peak at −0.4 V versus Ag/AgCl was observed (blue line). This can be attributed to the binding of MB to accessible guanine bases in the immobilized PNA probe. The MB peak current

https://dx.doi.org/10.1021/acs.analchem.0c04283
Anal. Chem. XXXX, XXX, XXX−XXX

decreased significantly following DNA hybridization owing to the duplex formation between the DNA and the immobilized acpcPNA probe that hinders the MB−guanine interaction. Because MB can act as an intercalator and may also bind to DNA via electrostatic interactions, some responses were still observed (yellow line). These results confirmed successful probe immobilization and DNA hybridization.

We further characterized the electrochemical behavior of the DNA sensor by measuring the charge transfer resistance (R_{ct}) using the EIS technique in the presence of $Fe(CN)_6^{3-/4-}$ with a concentration of 5 mM in 0.1 M PBS as a redox probe. All EIS Nyquist plots were fitted with the Randles equivalent circuit. As depicted in Figure 2B, the R_{ct} of the bare electrode was determined to be 1500 Ω. Once the acpcPNA probe was immobilized on the NC, an increase in R_{ct} to 1711 Ω was observed. This result confirmed that the acpcPNA probe was successfully immobilized on the electrode, resulting in the hindrance of electron transfer. Likewise, a further increase in the R_{ct} to 1800 Ω was observed after DNA hybridization with the PNA probe. However, when gold was metallized on the DNA structure, R_{ct} decreased to 873.4 Ω, which was explained by the superior electron conductivity of the system. Furthermore, the presence of the gold-metallized DNA was also characterized by SEM. As shown in Figure 2C, the deposition of AuNPs within the porous structure of the LFA paper device was observed after the electrodeposition step, which further supports the proposed sensing mechanism.

Optimization. *Influence of Device Geometry.* To achieve maximum response toward DNA metallization, the effects of varying the device geometries (with different channel widths and number of baffles) were studied.

First, by varying the shape and width of the detection zone (2, 2 mm with a chamber, and 3 mm), different SWV peak currents were obtained. As illustrated in Figure 3A(i), a channel width of 3 mm provided the highest current density among the three different device geometries. This behavior can be explained by the rate of the solution flow. In practice, a narrower channel width typically provides a faster flow rate (see Figure S5). However, this rapid flow rate may have a negative impact on DNA hybridization and electrostatic binding between Au^{3+} and the phosphate backbone of DNA, thus resulting in a lower current density. Hence, a channel width of 3 mm was chosen in this study.

Additionally, the effect of the number of baffle lines on the migration time of Au^{3+} was also investigated. As presented in Figure 3A(ii), the current difference (ΔI) increased with an increasing number of baffles up to four and then decreased rapidly after this point. It should be noted that a backflush of a fluidic stream from a nondelayed channel to the delayed channel was observed when more than four baffles were incorporated into the channel, therefore reducing the amount of Au^{3+} passing through to the detection zone. As a result, the four-baffle design was chosen as the optimal device structure.

Assay Conditions. In this part, a series of assay conditions (including the concentration of the acpcPNA probe, Au^{3+}, SDS, the detection and deposition time, and the deposition potential) were optimized. For the concentration of the acpcPNA probe [as shown in Figure 3B(i)], the SWV signal response (ΔI) increased with increasing acpcPNA concentration of up to 1000 nM. However, the current response decreased when the concentration of the acpcPNA probe was higher than 1000 nM. The overwhelming amounts of the acpcPNA probe can result in a probe density that is too high, which may eventually lower the electron transfer process between the gold and the electrode. Consequently, an acpcPNA probe concentration of 1000 nM was assigned as the optimal condition.

For the concentration of Au^{3+} [Figure 3B(ii)], it was observed that the electrochemical signal increased with increasing Au^{3+} concentration (ranging from 100 ppm to the maximum stock concentration of 1000 ppm). It is expected that an excess concentration of Au^{3+} can provide a large number of gold−DNA complexes (particularly in real DNA samples containing an extended DNA strand). Therefore, the optimal concentration of Au^{3+} was set at 1000 ppm.

Additionally, because of a limited steady-flow period, the influence of the assay time was studied [Figure 3B(iii)]. First, the effect of the detection time was investigated under a control experiment (deposition time of 120 s and deposition potential of −0.2 V vs Ag/AgCl) ranging from 6 min (4 min of the complete solution flowing to the detection zone and 2 min of deposition time) to 10 min. Within the studied time range, the largest current response was obtained at 7 min, which can provide the maximum binding between the acpcPNA probe-target DNA-Au^{3+} complex. It should be noted that the current signal decreased after 7 min. This and subsequent time points were beyond the quasi-steady regime; hence, the decrease in convective mass transfer and current response is to be expected. Therefore, the detection time was set at 7 min in further experiments.

In addition, the effect of surfactants was tested because they are widely used in biological assays, primarily as washing agents to reduce nonspecific adsorption and minimize the background signal.[33] Different types of surfactants, including Tween-20 (nonionic surfactant), sodium dodecyl sulfate (SDS, anionic surfactant), and hexadecyltrimethylammonium bromide (CTAB, cationic surfactant), were examined. As shown in Figure S6A, the background current decreased when 0.5% Tween-20 or 0.5% SDS was included in the running buffer (PBS) compared to that without the surfactant. This clearly shows the crucial role of the surfactant in preventing nonspecific adsorption. Note that an overlapping peak due to gold metal oxidation at 0.8 V versus Ag/AgCl with the background response was observed when 0.5% CTAB was added to the system (Figure S6B), which shows that CTAB is an unsuitable surfactant for this system. Comparing the current response difference (ΔI) between Tween-20 and SDS (Figure S6C), it was observed that the SDS system provided the highest response. It should be noted that the SDS concentration used in the present study was greater than the aqueous critical micelle concentration (CMC) of SDS (8 mM); therefore, the micellar phase was formed.[34] Interestingly, it was previously reported in the literature that the SDS micelle can behave as a soft template for the enlargement of AuNPs[35,36] and serve as a stabilizer for AuNPs.[37,38] Accordingly, SDS was selected as the optimal surfactant for the present study. In parallel, we also studied the effect of SDS concentration. As shown in Figure 3B(iv), the current response at concentrations above the CMC value (>0.3% w/v) was higher compared to that for concentrations below the CMC level and reached the maximum response at 0.5% w/v. This result evidently supports the function of the micellar SDS, whereby it can facilitate the gold metallization process on the electrode surface. Note that a concentration of SDS higher than 0.5% w/v can lead to solution leakage owing to the dissolution of the wax channel by the surfactant, leading to an

https://dx.doi.org/10.1021/acs.analchem.0c04283
Anal. Chem. XXXX, XXX, XXX−XXX

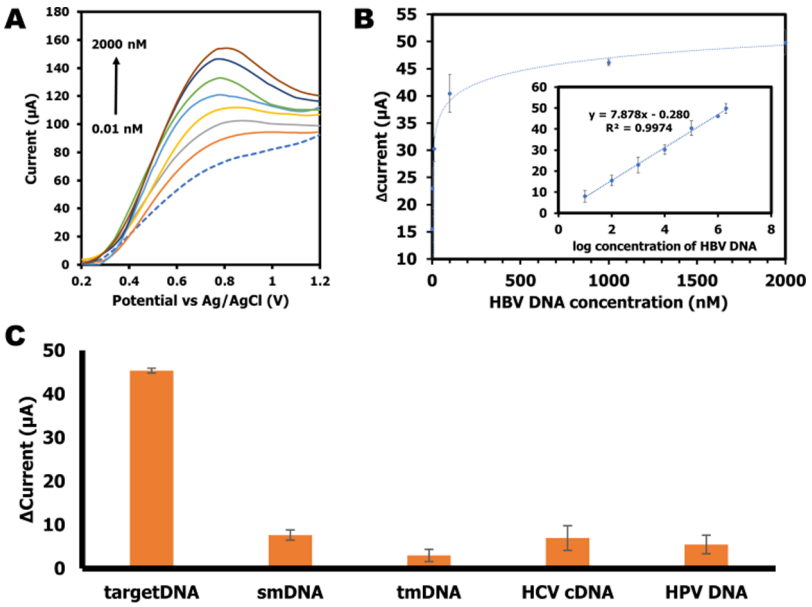


Figure 4. Anodic stripping voltammograms (A) and a plot of the current difference (ΔI: 10−50 μA) as a function of HBV DNA concentration (B), and the inset showing a linear calibration plot for ΔI vs logarithmic concentration of HBV DNA in the range of 10 pM to 2 μM (n = 3). (C) Selectivity of the proposed method (smDNA: single-base mismatch DNA, tmDNA: two-base mismatch DNA, HCV cDNA: hepatitis C virus cDNA, and HPV DNA: human papillomavirus DNA) (n = 3).

uncontrollable solution flow. Thus, 0.5% w/v of SDS solution was chosen as the optimal concentration for this system.

The deposition potential and the deposition time for the gold metallization step were optimized next. As illustrated in Figure 3B(v,vi), the highest response was achieved at a deposition potential of −0.2 V versus Ag/AgCl and a deposition time of 120 s. It is expected that a lower deposition potential (lower than −0.2 V vs Ag/AgCl) and a higher deposition time can result in a negative impact on the formation of nanoscale gold particles and inherently reduce the SWV response.[39] Based on these results, a deposition potential of −0.2 V versus Ag/AgCl and a deposition time of 120 s were chosen as the optimal conditions for the gold metallization step.

Analytical Performance of the Device for HBV DNA Detection. As shown in Figure 4A, the proposed eLFA device exhibits a sensitive response toward the HBV DNA target under the optimal conditions, that is, channel width = 3 mm, number of baffles = 4, acpcPNA probe concentration = 1000 nM, Au^{3+} concentration = 1000 ppm, type and concentration of the surfactant = 0.5% w/v SDS, detection time = 7 min, and deposition time = 120 s at a potential of −0.2 V versus Ag/AgCl. Note that a small shoulder peak due to nonspecific gold adsorption was still observed (dashed line), possibly attributed to the coordination interaction between Au metal and the N and O atoms of the nitrogenous bases and the amide backbone of the PNA probe.[26] Furthermore, the current signal for the Au-metallized DNA increased linearly with increasing logarithmic concentration of HBV DNA in the range of 10 pM to 2 μM (Figure 4B). The linear equation for the calibration plots was $y = 7.878(\log[\mathrm{DNA}_{(\mathrm{nM})}]) - 0.280$ with an R^2 of 0.9974. The limit of detection was calculated to be 7.23 pM (3SD/Slope). Compared to previous studies (Table S2), this innovative device presented a distinguished LOD with a superior dynamic range. Moreover, the overall assay can be rapidly performed within 7 min following a single manipulation (sample loading), whereas other related sensors require at least 30 min to accomplish the assay. Thus, this eLFA offers great potential for simple, rapid, and on-site HBV DNA detection of real clinical samples.

To evaluate the specificity of this DNA sensing, the current response toward four control DNA sequences with a concentration of 1 μM, including single-base mismatch DNA, two-base mismatch DNA, hepatitis C virus complementary DNA (cDNA) (HCV cDNA), and human papillomavirus DNA type 16 (HPV DNA), was studied. As presented in Figure 4C, the results indicate that the sensor can precisely distinguish complementary HBV DNA from other DNA sequences. Even the single-base mismatch DNA can be clearly discriminated from the target HBV DNA. The negligible response from the control groups demonstrates the excellent specificity of the proposed eLFA sensor, which can be attributed to the high specificity of the acpcPNA probe.

Furthermore, the DNA sensing device demonstrated good accuracy and repeatability with an RSD of 10.3% for five independent devices. Moreover, the DNA test strip stored at 4 °C maintained its performance for up to 1 month (defined as a retention of 90−110% of the initial response), indicating satisfactory stability (Figure S7).

Human Serum Sample Analysis. To further verify the applicability of the developed eLFA DNA sensor for clinical diagnosis, HBV DNA extracted from serum of the patients was quantified and compared with the standard real-time PCR method. In this work, denaturation of the DNA sample was not necessary prior to the hybridization on the eLFA device. It was known from previous studies that the acpcPNA probe can invade double-stranded DNA at least under low salt conditions.[40] It is also possible that the presence of SDS in the buffer helps destabilizing the DNA−DNA duplex, thus further facilitating PNA binding. Typically, a calibration plot to estimate an unknown DNA concentration in the real-time PCR assay is created from the plasmid DNA construct carrying the HBV DNA as the standard.[41] To construct the calibration graph, the plasmid standard was serially diluted to generate a

https://dx.doi.org/10.1021/acs.analchem.0c04283
Anal. Chem. XXXX, XXX, XXX−XXX

range of concentrations for subsequent electrochemical detection. Using the eLFA device, a linear relationship between the current response and the logarithm of the plasmid concentration in the range of 10^2 to 10^6 copies μL^{-1} (R^2 = 0.9955) was established, as shown in Figure S8. This calibration graph was used to quantify the HBV DNA from the patients' serum. As summarized in Table 1, HBV DNA in the real sample can be detected and quantified from the extracted DNA sample without requiring additional DNA amplification methods (such as PCR). Furthermore, the results obtained from electrochemical detection using the proposed eLFA method were in good agreement with the standard real-time PCR approach (using a paired *t*-test statistical method) with a percentage error of 3.5 or less. These results together with the ultraperformance (including the fast analysis time and fully automated platform) clearly indicated that the proposed eLFA DNA sensor is technically sound and applicable for detection of the real DNA sample with high reliability and accuracy.

Table 1. Results for Real HBV DNA Detection from Patients Using the Proposed Device Compared with the Real-Time PCR Method

	real-time PCR[a]	eLFA device[a] (mean ± SD)	% error
sample 1	5.39	5.44 ± 0.34	0.93
sample 2	5.44	5.63 ± 0.06	3.50
sample 3	5.27	5.20 ± 0.11	1.32

[a]Log copies μL^{-1}.

CONCLUSIONS

In summary, we present an automated lateral flow electrochemical device for signal-on detection of hepatitis B virus DNA employing a gold metallization detection strategy. acpcPNA, which was effortlessly immobilized on a lateral flow test strip, can function as a selective probe to capture the incoming HBV DNA target. The use of the PNA probe not only offers high specificity but also contributes to lowering the background response usually observed in traditional DNA metallization sensors. The gold-metallized PNA-DNA complex exhibited a notable signal enhancement, thus enabling direct detection of HBV DNA without requiring PCR or other types of DNA amplification. The multiple steps in the lateral flow assay were enabled in a time-sequenced fashion using a time-delayed microfluidic channel fabricated via a wax-printing method. With this design, the overall assay was carried out by a single operation of sample loading and took only 7 min to complete without sacrificing the sensing performance. The eLFA sensor exhibited an LOD of 7.23 pM and a wide linearity range between 10 pM and 2 μM (6 orders of magnitude). In serum samples of patients, our results were in accordance with values obtained from the gold standard real-time PCR method. With outstanding analytical performance in terms of ease of use, rapidity, sensitivity, and selectivity, this sensor can serve as an excellent prototype for other biological assays (e.g., bacteria or virus detection) that require multiple operations to be performed in a time-sequenced fashion.

ASSOCIATED CONTENT

Supporting Information

The Supporting Information is available free of charge at https://pubs.acs.org/doi/10.1021/acs.analchem.0c04283.

DNA sequences used in this study, comparison with the previous electrochemical approach for HBV DNA detection, mass spectrum of the acpcPNA, chromatogram for confirming the purity of acpcPNA, component of the automated paper-based lateral flow device, amperometric response of ascorbic acid, flow velocity at different channel widths, effect of the type of surfactants, stability of the automated eLFA device, plasmid construct HBV DNA preparation, and feasibility of the proposed device with the HBV DNA plasmid constructs (PDF)

Device operation (AVI)

Study of flow velocity (AVI)

AUTHOR INFORMATION

Corresponding Author

Orawon Chailapakul − *Electrochemistry and Optical Spectroscopy Center of Excellence (EOSCE), Department of Chemistry, Faculty of Science, Chulalongkorn University, Bangkok 10330, Thailand;* orcid.org/0000-0002-2151-7370; Email: corawon@chula.ac.th

Authors

Chawin Srisomwat − *Electrochemistry and Optical Spectroscopy Center of Excellence (EOSCE), Department of Chemistry, Faculty of Science, Chulalongkorn University, Bangkok 10330, Thailand*

Abdulhadee Yakoh − *Electrochemistry and Optical Spectroscopy Center of Excellence (EOSCE), Department of Chemistry, Faculty of Science, Chulalongkorn University, Bangkok 10330, Thailand;* orcid.org/0000-0002-8392-5492

Natthaya Chuaypen − *Center of Excellence in Hepatitis and Liver Cancer, Department of Biochemistry, Faculty of Medicine, Chulalongkorn University, Bangkok 10330, Thailand*

Pisit Tangkijvanich − *Center of Excellence in Hepatitis and Liver Cancer, Department of Biochemistry, Faculty of Medicine, Chulalongkorn University, Bangkok 10330, Thailand*

Tirayut Vilaivan − *Organic Synthesis Research Unit, Department of Chemistry, Faculty of Science, Chulalongkorn University, Bangkok 10330, Thailand*

Complete contact information is available at: https://pubs.acs.org/10.1021/acs.analchem.0c04283

Author Contributions

C.S.: conceptualization, methodology, investigation, and writing—original draft and visualization. A.Y.: conceptualization, methodology, and writing—review and editing. N.C.: resources and writing—review and editing. P.T.: resources. T.V.: resources and writing—review and editing. O.C.: supervision and writing—review and editing and funding acquisition.

Notes

The authors declare no competing financial interest.

ACKNOWLEDGMENTS

This research was partially supported by the National Research Council of Thailand (NRCT) through the Royal Golden Jubilee Ph.D. program (grant number PHD/0016/2561). The authors also thank the Center of Excellence in Hepatitis and

Liver Cancer, Department of Biochemistry, Faculty of Medicine, Chulalongkorn University, and Thailand Research Fund (RTA6280004) for providing the real HBV DNA samples in serum and preparing the HBV plasmid. O.C. and C.S. would like to thank the 90th Anniversary of Chulalongkorn University, Rachadapisek Sompote Fund for the financial support.

REFERENCES

(1) Xu, Y.; Wei, Y.; Cheng, N.; Huang, K.; Wang, W.; Zhang, L.; Xu, W.; Luo, Y. *Anal. Chem.* **2018**, *90*, 708−715.
(2) Zhang, J.; Shen, Z.; Xiang, Y.; Lu, Y. *ACS Sens.* **2016**, *1*, 1091−1096.
(3) Gehrke, T.; Lausmann, C.; Citak, M.; Bonanzinga, T.; Frommelt, L.; Zahar, A. *J. Bone Jt. Surg.* **2018**, *100*, 42.
(4) Sajid, M.; Kawde, A.-N.; Daud, M. *J. Saudi Chem. Soc.* **2015**, *19*, 689−705.
(5) Jeong, S.-G.; Kim, J.; Jin, S. H.; Park, K.-S.; Lee, C.-S. *Korean J. Chem. Eng.* **2016**, *33*, 2761−2770.
(6) Preechakasedkit, P.; Siangproh, W.; Khongchareonporn, N.; Ngamrojanavanich, N.; Chailapakul, O. *Biosens. Bioelectron.* **2018**, *102*, 27−32.
(7) Sinawang, P. D.; Rai, V.; Ionescu, R. E.; Marks, R. S. *Biosens. Bioelectron.* **2016**, *77*, 400−408.
(8) Pellitero, M. A.; Kitsara, M.; Eibensteiner, F.; del Campo, F. J. *Analyst* **2016**, *141*, 2515−2522.
(9) Dempsey, E.; Rathod, D. *IEEE Sensor. J.* **2018**, *18*, 1828−1834.
(10) Rapisarda, V.; Loreto, C.; Malaguarnera, M.; Ardiri, A.; Proiti, M.; Rigano, G.; Frazzetto, E.; Ruggeri, M. I.; Malaguarnera, G.; Bertino, N.; Malaguarnera, M.; Catania, V. E.; Di Carlo, I.; Toro, A.; Bertino, E.; Mangano, D.; Bertino, G. *World J. Hepatol.* **2016**, *8*, 573.
(11) Idrees, H. A.; Al Fadhil, A. O.; Waggas, A. E. *Afr. J. Med. Sci.* **2017**, *2*, 7.
(12) Song, J. E.; Kim, D. Y. *Ann. Transl. Med.* **2016**, *4*, 338.
(13) Niemz, A.; Ferguson, T. M.; Boyle, D. S. *Trends Biotechnol.* **2011**, *29*, 240−250.
(14) Toyama, M.; Sakakibara, N.; Takeda, M.; Okamoto, M.; Watashi, K.; Wakita, T.; Sugiyama, M.; Mizokami, M.; Ikeda, M.; Baba, M. *Virus Res.* **2019**, *271*, 197677.
(15) Lall, S.; Choudhary, M. C.; Mahajan, S.; Kumar, G.; Gupta, E. *Virus Dis.* **2019**, *30*, 186−192.
(16) Tao, F.; Fang, J.; Guo, Y.; Tao, Y.; Han, X.; Hu, Y.; Wang, J.; Li, L.; Jian, Y.; Xie, G. *Anal. Biochem.* **2018**, *554*, 16−22.
(17) Srisomwat, C.; Teengam, P.; Chuaypen, N.; Tangkijvanich, P.; Vilaivan, T.; Chailapakul, O. *Sens. Actuators, B* **2020**, *316*, 128077.
(18) Wang, J.; Rincón, O.; Polsky, R.; Dominguez, E. *Electrochem. Commun.* **2003**, *5*, 83−86.
(19) Jampasa, S.; Siangproh, W.; Laocharoensuk, R.; Yanatatsaneejit, P.; Vilaivan, T.; Chailapakul, O. *Sens. Actuators, B* **2018**, *265*, 514−521.
(20) Cinti, S.; Cinotti, G.; Parolo, C.; Nguyen, E. P.; Caratelli, V.; Moscone, D.; Arduini, F.; Merkoci, A. *Anal. Chem.* **2019**, *92*, 1674−1679.
(21) Vilaivan, T. *Acc. Chem. Res.* **2015**, *48*, 1645−1656.
(22) Fang, Z.; Kelley, S. O. *Anal. Chem.* **2009**, *81*, 612−617.
(23) Kong, J.; Ferhan, A. R.; Chen, X.; Zhang, L.; Balasubramanian, N. *Anal. Chem.* **2008**, *80*, 7213−7217.
(24) Mao, X.; Liu, S.; Yang, C.; Liu, F.; Wang, K.; Chen, G. *Anal. Chim. Acta* **2016**, *909*, 101−108.
(25) Vilaivan, T.; Srisuwannaket, C. *Org. Lett.* **2006**, *8*, 1897−1900.
(26) Chen, Z.; Liu, C.; Cao, F.; Ren, J.; Qu, X. *Chem. Soc. Rev.* **2018**, *47*, 4017−4072.
(27) Yakoh, A.; Chaiyo, S.; Siangproh, W.; Chailapakul, O. *ACS Sens.* **2019**, *4*, 1211−1221.
(28) Adkins, J. A.; Noviana, E.; Henry, C. S. *Anal. Chem.* **2016**, *88*, 10639−10647.
(29) Brett, C. M. A.; Lima, J. L. F. C.; Garcia, M. B. Q. *Analyst* **1994**, *119*, 1229−1233.
(30) Washburn, E. W. *Phys. Rev.* **1921**, *17*, 273−283.
(31) Kerman, K.; Ozkan, D.; Kara, P.; Meric, B.; Gooding, J. J.; Ozsoz, M. *Anal. Chim. Acta* **2002**, *462*, 39−47.
(32) Torati, S. R.; Reddy, V.; Yoon, S. S.; Kim, C. *Biosens. Bioelectron.* **2016**, *78*, 483−488.
(33) Smith, L.; Burgoyne, L. *BMC Ecol.* **2004**, *4*, 4.
(34) González-Romero, E.; Fernández-Calvar, M. B.; Bravo-Díaz, C. *Langmuir* **2002**, *18*, 10311−10317.
(35) Wang, W.; Yuan, X.; Zhang, W.; Gao, Q.; Qi, H.; Zhang, C. *Electrochim. Acta* **2012**, *78*, 377−383.
(36) Bakshi, M. S.; Kaur, G.; Thakur, P.; Banipal, T. S.; Possmayer, F.; Petersen, N. O. *J. Phys. Chem. C* **2007**, *111*, 5932−5940.
(37) Navarro-Badilla, A.; Hurtado, R. B.; Cortez-Valadez, M.; Perez-Rodriguez, A.; Flores-Acosta, M.; Maldonado-Arce, A. *Phys. E* **2017**, *87*, 93−97.
(38) Cabrera, G. F. S.; Balbin, M. M.; Eugenio, P. J. G.; Zapanta, C. S.; Monserate, J. J.; Salazar, J. R.; Mingala, C. N. *Biochem. Biophys. Res. Commun.* **2017**, *484*, 774−780.
(39) Schmid, G. M.; Bolger, G. W. *Clin. Chem.* **1973**, *19*, 1002−1005.
(40) Bohländer, P. R.; Vilaivan, T.; Wagenknecht, H.-A. *Org. Biomol. Chem.* **2015**, *13*, 9223−9230.
(41) Sivaganesan, M.; Seifring, S.; Varma, M.; Haugland, R. A.; Shanks, O. C. *BMC Bioinf.* **2008**, *9*, 120.

https://dx.doi.org/10.1021/acs.analchem.0c04283
Anal. Chem. XXXX, XXX, XXX−XXX